Desalination and Water Treatment
www.deswater.com
doi: 10.5004/dwt.2020.24940

178 (2020) 101–109
February

Adsorption of phosphate on Ca-carbon foam: batch experiments and model evaluation

Juryeon Oh[a], Chuntak Phark[a], Seungho Jung[a], Jechan Lee[a], Kwon-Young Choi[a,*], Chang-Gu Lee[a,*], Seong-Jik Park[b], Sang-Hyup Lee[c,*]

[a]*Department of Environmental and Safety Engineering, Ajou University, Suwon 16499, Korea, Tel. +82 31 219 2405; emails: kychoi@ajou.ac.kr (K.-Y. Choi), changgu@ajou.ac.kr (C.-G. Lee), dhwnfus@naver.com (J. Oh), phark.c.t@gmail.com (C. Phark), processsafety@ajou.ac.kr (S. Jung), jlee83@ajou.ac.kr (J. Lee)*
[b]*Department of Bioresources and Rural Systems Engineering, Hankyong National University, Anseong 456–749, Korea, email: parkseongjik@hknu.ac.kr (S.-J. Park)*
[c]*Center for Water Resource Cycle Research, Korea Institute of Science and Technology, Seoul 136–791, Korea, email: yisanghyup@kist.re.kr (S.-H. Lee)*

Received 12 April 2019; Accepted 21 September 2019

ABSTRACT

Phosphate, which can cause eutrophication of the aquatic environment, can be effectively removed by an adsorption process using calcium-containing adsorbents. In this study, Ca-carbon foam was prepared by a simple method that entailed addition of Ca during the manufacturing process of carbon foam, and the phosphate removal characteristics of the prepared foam were analyzed using kinetic, equilibrium isotherm, and artificial neural network (ANN) models. The phosphate adsorption capacity decreased with an increase in the solution pH from 3.05 to 6.99. Furthermore, phosphate adsorption increased with increasing time, and the kinetic data were found to be well described by a pseudo-second-order model. The Freundlich isotherm provided the best fit of the equilibrium data, which indicates multilayer adsorption of phosphate on the Ca-carbon foam. The phosphate adsorption capacity as a function of three operational parameters—solution pH, initial phosphate concentration, and time—was well predicted by an ANN model ($R^2 > 0.993$), and the optimal ANN for the process of phosphate adsorption on Ca-carbon foam had a 3–20–1 structure with 20 hidden layers. The solution pH was the most influential operational parameter out of all the examined parameters. The results of these analyses are expected to be useful in designing the process of phosphate adsorption from aqueous solutions.

Keywords: Phosphate; Carbon foam; Kinetic adsorption model; Equilibrium isotherm; Artificial neural network

1. Introduction

Phosphorus is an essential nutrient for plant growth; however, its presence in excessive amounts in the aquatic environment is a cause of concern because it can induce eutrophication of water bodies [1,2]. Therefore, various physical, chemical, and biological methods have been applied to reduce the phosphorus concentration of effluents prior to discharge [3]. In particular, adsorption is the most effective and widely used technique for removal of phosphorus from water because of its simple concept, convenient implementation, and low cost [4]. In recent years, several researchers have reported stable and enhanced phosphate removal performance of calcium-modified adsorbents [5,6]. In fact,

* Corresponding authors.

calcium has been widely used as a way to remove phosphorus through calcium-phosphate precipitation due to its low cost. Thus, functionalization of the adsorbent using calcium can be a way to increase its ability to remove phosphate [6].

Carbon foam is a sponge-like carbon material that has a large surface area because of its open cell structure [7]. On account of its excellent strength and thermal and electrical properties, it has been employed for various purposes, for example, as a refractory insulation material, filter for corrosive chemicals, porous electrode, and acoustic absorber [8,9]. Carbon foam can be easily manufactured by an inexpensive method, that is, carbonization of phenolic foam [10,11], and it can be easily modified by adjusting the additives during its preparation process. Lee et al. [12] modified carbon foam with Fe_2O_3 to remove chromium, copper, and nickel from industrial plating wastewater. Similarly, although calcium-containing carbon foam can be easily manufactured, there has been no study using it to remove phosphorus from aqueous solution.

Two basic components of the adsorption process—equilibrium and kinetics—must be analyzed in order to understand this process clearly. Equilibrium provides an understanding of adsorption capacity, whereas kinetics provides insight into possible pathways of an adsorption [13,14]. A number of theoretical models and equations have been used for this purpose, and the best fit of experimental data has been interpreted to provide appropriate information on the adsorption process through design parameters [15,16]. These parameters are important in designing an actual adsorption treatment plant to remove different contaminants from water [14,15,17]. Furthermore, in recent years, artificial neural network (ANN) models have been used to predict the outcome of the adsorption process with reasonable certainty and speed [18]. An ANN is a computer simulation technique that essentially mimics the human brain, and it is used to identify complex input–output relationships and predict results from input data [19]. Several researchers have applied the ANN model to predict the results of various adsorption studies, such as phosphorus adsorption on red mud and phenol adsorption on carbon-based adsorbents [20,21]. In addition, the importance of different operational parameters was quantified [20].

Therefore, in this study, the characteristics of phosphate adsorption on Ca-carbon foam were analyzed using kinetic, equilibrium isotherm, and ANN models. The adsorption of phosphate was tested under different operational parameters, that is, solution pH, time, and initial phosphate concentration. Pseudo-first-order, pseudo-second-order, and Elovich models were used for kinetic data analysis. Furthermore, the Freundlich, Langmuir, and Redlich–Peterson isotherms were employed for equilibrium data analysis. Finally, the relative importance of the different operational parameters for phosphate adsorption on Ca-carbon foam was predicted by the ANN model.

2. Materials and methods

2.1. Materials

Potassium dihydrogen phosphate (KH_2PO_4) was used to prepare a phosphate stock solution (1,000 mg/L as PO_4–P). Reagent-grade HCl and NaOH were used for pH adjustment of the solution, and ultrapure water (deionized [DI] water, 18.2 MΩ/cm) was used for all dilutions and reagent preparations.

2.2. Adsorbent

Phenolic resin-based carbon foam was supplied from Smithers-Oasis Korea Co. Ltd. and the preparation method has been described in detail in previous studies [10,12]. Briefly, the phenolic resin (1.0 kg) was synthesized in a laboratory via compounding of formaldehyde (1.5 kg) and a base catalyst (40 g). The mixture was neutralized (pH 6–7) using dilute sulfuric acid, and the moisture content (9%) was adjusted through dehydration under vacuum. Then, an alkyl-ether-type surfactant (2.0 g) was mixed with the prepared phenolic resin, and an organic acid curing agent (80 g) containing calcium carbonate (100 g) was added to the mixture to prepare the Ca-carbon foam. A hydrocarbon foaming agent (20 g) was also added to the mixture, and the resulting mixture was stirred thoroughly in a mold. The synthesized foam was aged in a convection oven. Subsequently, the dried phenolic foam was carbonized at 900°C under N_2 atmosphere [10,12]. The synthesized Ca-carbon foam was uniformly pulverized (≈75 μm) using mortar prior to the adsorption experiments.

2.3. Adsorption studies

A series of phosphate adsorption experiments were performed under batch conditions to investigate the effects of different operational parameters on the adsorption performance of the Ca-carbon foam. As listed in Table 1, the solution pH, time, and initial phosphate concentration were the considered operational parameters. The pH experiment was performed at solution pH values of 2, 3, 4, 5, 6, and 7. The solution pH was adjusted with 1 M HCl and 1 M NaOH. Kinetic adsorption tests were conducted for times of 10, 20,

Table 1
Ranges of operational parameters for ANN analysis

Variable	Operational parameter	Range
Input layer	Solution pH	1.97–6.99
	Time, min	10–120
	Initial phosphate concentration, mg/L	50–250
Output layer	Phosphate adsorption capacity, mg/g	0–54.159
Total number of data points		38

30, 45, 60, 90, and 120 min by using 100 mg/L (as PO_4–P) of pH 3 phosphate solution. The effect of the initial phosphate concentration on its adsorption was tested using 50, 75, 100, 150, 200, and 250 mg/L (as PO_4–P) phosphate solutions with a time of 120 min. The experiments were performed using a rotary shaker (MG-150D, Mega Science, Korea) at 25 rpm at 21°C ± 2°C. The adsorbent dose added to the solution was 2.5 g/L. After the adsorption, sampling was performed using a 0.45 μm filter (Whatman, USA), and the residual phosphate concentration as PO_4–P was measured using an inductively coupled plasma-optical emission spectrometer (Prodigy ICP, Teledyne Leeman Labs, USA). The phosphate adsorption capacity per unit mass of the adsorbent was calculated as follows:

$$q = \frac{C_i - C_f}{a} \tag{1}$$

where C_i and C_f are the concentrations of a contaminant in the aqueous phase before and after the adsorption (mg/L), respectively; and a is the dose of Ca-carbon foam (g/L). The pH of the solution was measured using a pH probe (8302BNUMD, ORION, USA). All the batch experiments were performed in triplicate.

2.4. ANN modeling

Three input parameters—pH, time, and initial phosphate concentration—were used for the ANN modeling. The nnstart function included in MATLAB R2018b was used to implement a three-layer feed-forward network with back-propagation learning for the modeling (Fig. 1). This network employed the tan-sigmoid (tansig) transfer function for the hidden layer and a linear transfer function (purelin) for the output layer. For this network, only one hidden layer was used. The Levenberg–Marquardt (trainlm) algorithm with 1,000 epochs was selected for training the functions for this network. The results of training were expressed in one neuron in the output layer as the adsorption capacity. The mean squared error (MSE) was used to evaluate the performance function of the network.

3. Results and discussion

3.1. Effect of solution pH on phosphate adsorption

The solution pH can significantly affect the adsorption of ionic contaminants [18,22]. Both the chemical species of the ionic contaminants and the surface charge of the adsorbent can change with the solution pH. In particular, the adsorption of anionic contaminants such as phosphate generally decreases as pH increases, on account of increased competition with hydroxyl ions [23,24]. On the other hand, contaminant removal via surface precipitation does not occur under low-pH conditions [6,25]. This tendency was also observed for the phosphate adsorption on the Ca-carbon foam in this study. As shown in Fig. 2a, the adsorption of phosphate peaked to 25.25 ± 1.31 mg/g at pH 3.05 and decreased to 16.79 ± 1.78 mg/g at pH 6.99. Phosphate removal was not observed at pH 1.97 due to calcium release from the adsorbent in acidic conditions (97.89 ± 2.21 mg/L). From analysis using the Visual MINTEQ 3.1 program (Fig. 2b), the monovalent form of phosphate ($H_2PO_4^-$) was found to be the dominant species under our experimental conditions.

3.2. Effects of time and initial phosphate concentration

Time is another important operational parameter in designing actual treatment facilities for removal of contaminants from water by the adsorption process [26]. The adsorption of phosphate on the Ca-carbon foam as a function of time is shown in Fig. 3a. The phosphate adsorption gradually increased with increasing time. The adsorption capacity increased from 6.17 ± 0.64 to 24.83 ± 0.01 mg/g with an increase in the time from 10 to 120 min. The removal

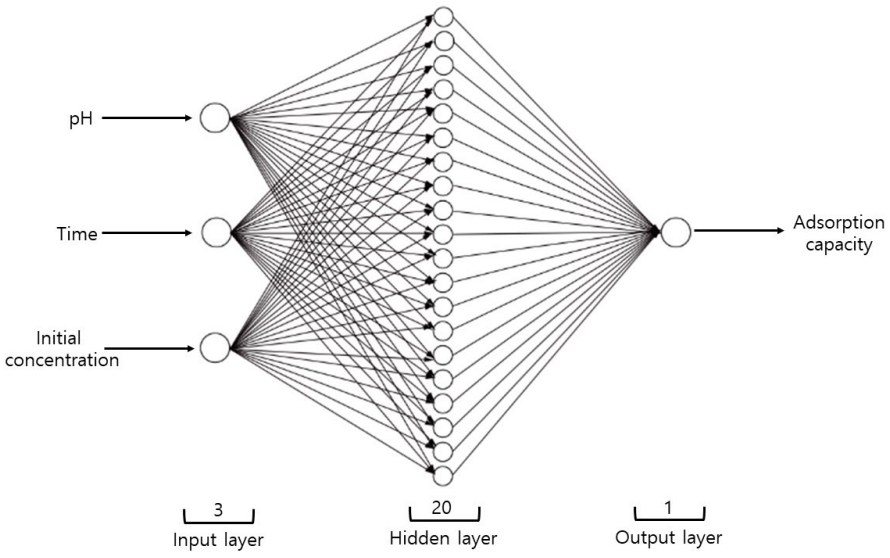

Fig. 1. Schematic architecture of (3–20–1) ANN model for adsorption process.

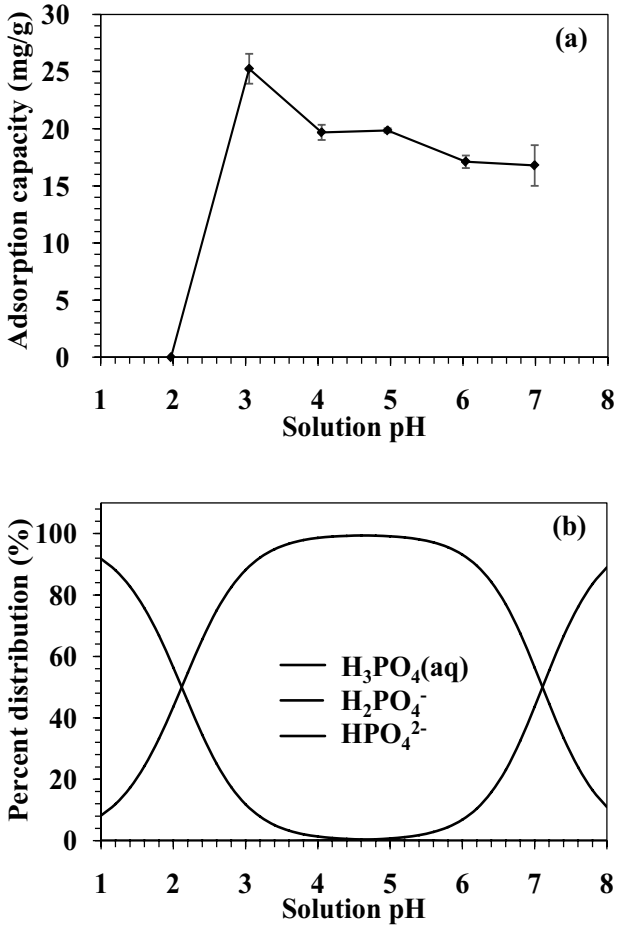

Fig. 2. Effects of solution pH on (a) phosphate adsorption capacity (initial phosphate concentration: 100 mg/L as PO_4–P, time: 2 h) and (b) distribution of phosphate species (calculated using Visual MINTEQ 3.1 program).

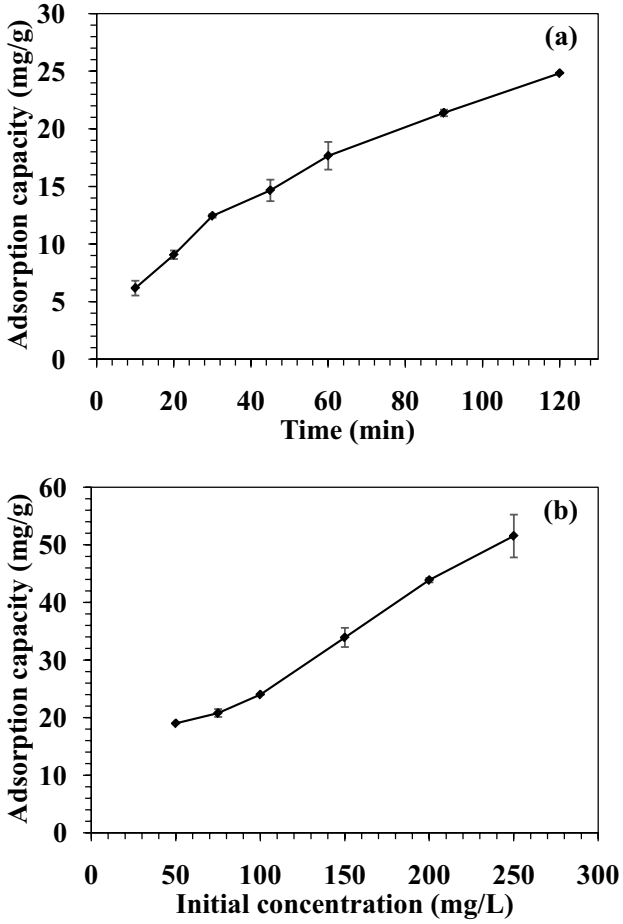

Fig. 3. Effects of (a) time and (b) initial phosphate concentration on adsorption (solution pH: 3).

percentage of phosphate was 62% (initial phosphate concentration: 100 mg/L as PO_4–P) for a time of 120 min.

The adsorption capacity of the adsorbent is typically determined via experiments with different initial concentrations of the adsorbate [27]. Therefore, the effect of the initial phosphate concentration (50–250 mg/L as PO_4–P) on phosphate adsorption was tested, and the results are shown in Fig. 3b. As the initial phosphate concentration increased, the phosphate adsorption capacity of the adsorbent increased from 19.02 ± 0.03 to 51.53 ± 3.72 mg/g whereas the removal percentage decreased from 95% to 52%. This increase in the adsorption capacity is due to the increased driving force for adsorption at the adsorption site on the adsorbent resulting from an increase in the adsorbate concentration [28,29]. Similar results were reported for phosphate adsorption on Ca-modified biochar and thermally modified Ca-rich attapulgite [6,30].

3.3. Adsorption kinetics

The adsorption data shown in Fig. 3a as a function of time were analyzed in order to determine the parameters of the pseudo-first-order [31] (Eq. (2)), pseudo-second-order [32] (Eq. (3)), and Elovich [33] (Eq. (4)) kinetic models:

$$q_t = q_e\left(1 - e^{-k_1 t}\right) \tag{2}$$

$$q_t = \frac{k_2 q_e^2 t}{1 + k_2 q_e t} \tag{3}$$

$$q_t = \frac{1}{\beta}\ln(\alpha\beta) + \frac{1}{\beta}\ln(t) \tag{4}$$

where q_t and q_e are the adsorbed amounts of phosphate at time t and equilibrium time (mg/g), respectively; k_1 and k_2 are the adsorption rate constants of the pseudo-first-order (1/min) and pseudo-second-order models (g/mg/min), respectively; and α and β are the initial adsorption rate constant (mg/g/min) and the Elovich adsorption constant (g/mg), respectively. The kinetic model parameters that minimize the sum of squared errors (SSE) for a given nonlinear equation were obtained using the Solver function in Microsoft Excel and are presented in Table 2 along with the calculated coefficient (R^2) for each model. In addition,

Table 2
Kinetic adsorption parameters obtained from model fitting to kinetic data

Pseudo-first-order model				Pseudo-second-order model				Elovich model			
q_e	k_1	R^2	SSE	q_e	k_2	R^2	SSE	α	β	R^2	SSE
(mg/g)	(1/min)			(mg/g)	(g/mg/min)			(mg/g/min)	(g/mg)		
26.395	0.020	0.986	5.032	36.405	4.5E-04	0.991	2.657	1.399	0.133	0.972	7.336

the nonlinear fitting of each model using the calculated parameters is shown in Fig. 4 together with the experimental data. From the model fittings and calculated parameters, it was found that all the kinetic models successfully replicated the experimental data, among which the pseudo-second-order model was most suitable for describing the experimental data (R^2 = 0.991, SSE = 2.657). This finding indicates that chemisorption is involved in the phosphate adsorption on the Ca-carbon foam [34]. Meanwhile, the expected adsorption capacity for the pseudo-second-order model at equilibrium time was 36.405 mg/g, which was higher than the expected value for the pseudo-first-order model at equilibrium time (26.395 mg/g). In addition, the adsorption rate constants of the pseudo-second-order model (k_2) could be used to calculate the initial adsorption rate constant (h) at $t \to 0$ by the following equation:

$$h = k_2 q_e^2 \tag{5}$$

The calculated value of h was 0.598 mg/g/min, which was lower than half the value of α (initial adsorption rate constant) of the Elovich model (1.399 mg/g/min).

3.4. Adsorption isotherms

Nonlinear forms of the Freundlich [35] (Eq. (6)), Langmuir [36] (Eq. (7)), and Redlich–Peterson [37] (Eq. (8)) isotherm models were employed to analyze the experimental data obtained as a function of the initial phosphate concentration, as depicted in Fig. 3b:

$$q_e = K_F C_e^{1/n} \tag{6}$$

$$q_e = \frac{Q_m K_L C_e}{1 + K_L C_e} \tag{7}$$

$$q_e = \frac{K_R C_e}{1 + a_R C_e^g} \tag{8}$$

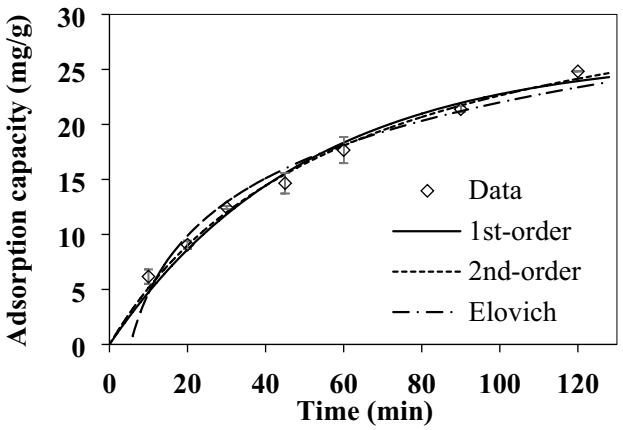

Fig. 4. Nonlinear fitting of kinetic models to experimental data. The model parameters are listed in Table 2.

where C_e is the equilibrium concentration of phosphate in the aqueous solution (mg/L); K_F and $1/n$ are the Freundlich constant related to the adsorption capacity (L/g) and the adsorption intensity, respectively; Q_m and K_L are the maximum adsorption capacity (mg/g) of the Ca-carbon foam and the Langmuir constant related to the affinity of the binding site (L/mg), respectively; K_R and a_R are the Redlich–Peterson constant related to the adsorption capacity (L/g) and the affinity of the binding site (L/mg), respectively; and g is the Redlich–Peterson constant related to the adsorption intensity. The parameters of the three nonlinear models were obtained using the Solver function in Microsoft Excel and are listed in Table 3, and the model fittings are shown in Fig. 5. The higher R^2 and lower SSE of the Freundlich and the Redlich–Peterson isotherms imply that both of these isotherms are more suitable than the Langmuir isotherm for describing the equilibrium data, which indicate multilayer adsorption of phosphate on the Ca-carbon foam [4,38]. As shown in Fig. 5, the fittings of the Freundlich and Redlich–Peterson isotherms coincide with each other, which means

Table 3
Equilibrium isotherm parameters obtained from model fitting to equilibrium data

Freundlich				Langmuir				Redlich–Peterson					
K_F	$1/n$	R^2	SSE	Q_m	K_L	R^2	SSE	K_R	a_R	K_R/a_R	g	R^2	SSE
(L/g)				(mg/g)	(L/mg)			(L/g)	(L/mg)	(mg/g)			
2.699	0.614	0.983	11.562	95.273	0.009	0.967	24.739	5330.970	1974.612	2.700	0.386	0.983	11.562

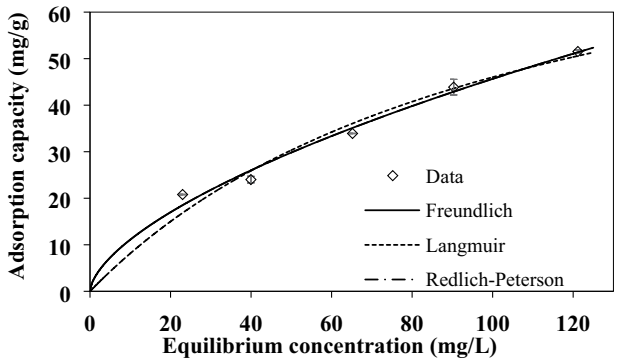

Fig. 5. Nonlinear fitting of adsorption isotherms to experimental data. The model parameters are listed in Table 3.

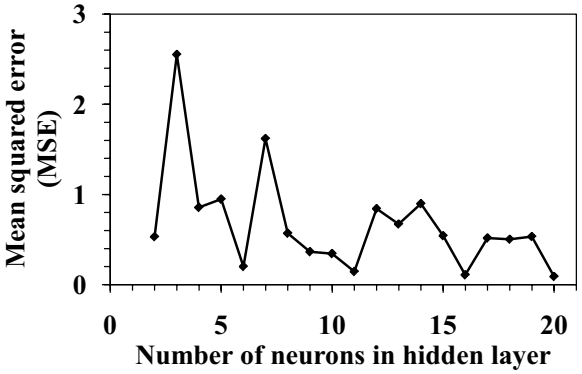

Fig. 6. Mean squared error (MSE) for different numbers of neurons in the single-hidden-layer ANN architecture.

that the two equations become identical when K_R and a_R are sufficiently larger than unity [39,40]. Thus, in Table 3, K_F corresponds well to the value of K_R/a_R, and $1/n$ coincides with $(1–g)$. A comparison of the Langmuir maximum adsorption capacities (Q_m) of Ca-containing adsorbents is presented in Table 4; it is seen that the phosphate (as PO_4–P) adsorption capacity of the Ca-carbon foam is comparable with the values reported in the literature (4.58–203.6 mg/g) [5,6,30,41].

3.5. Predictive modeling using ANN

In order to achieve an optimal network, the number of neurons in the hidden layer was set within the range of 2–20 for performing training. The MSE changed with the number of neurons in the hidden layer (Fig. 6). The MSE had the lowest value (0.090) when the number of neurons in the hidden layer was 20. Thus, the optimal ANN consists of an input layer with 3 neurons, a hidden layer with 20 neurons, and an output layer with 1 neuron, which can be expressed as a (3–20–1) ANN model. A total of 38 samples were randomly divided to examine the correlation between the normalized predicted adsorption capacity and normalized experimental data for training, testing, and validation and the correlation between all normalized predicted data and all normalized experimental data on the adsorption capacity. The ANN used 70% data (26 samples) for training, 15% data (6 samples) for testing, and 15% data (6 samples) for validation and showed a high correlation ($R^2 > 0.993$) between the experimental and predicted data (Fig. 7); this confirms the applicability of the ANN model with the trainlm algorithm to the prediction of phosphate adsorption on Ca-carbon foam.

The correlation of the output of the model to its input is expressed as follows:

$$\text{Output} = \text{purelin}\left(\text{LW} \times \text{tansig}\left(\text{IW} \times \left\{x(1); x(2); x(3)\right\} + b_1\right) + b_2\right) \tag{9}$$

where $x(1)$, $x(2)$, and $x(3)$ are inputs; IW and b_1 are the weight and bias, respectively, of the hidden layer; and LW and b_2 are the weight and bias, respectively, of the output layer. The weight and bias values obtained for the optimally trained ANN are listed in Table 5. Sensitivity analysis was performed in order to estimate the relative importance of each input parameter affecting the results; specifically, the relative importance was determined by calculating the connection weights according to the following equation [42,43]:

$$V = \frac{\sum_{j=1}^{h}\left[\frac{|\text{IW}_{ij}|}{\sum_{k=1}^{m}|\text{IW}_{jk}|} \times |\text{LW}_j|\right]}{\sum_{k=1}^{m}\left[\sum_{j=1}^{h}\left[\frac{|\text{IW}_{ij}|}{\sum_{k=1}^{m}|\text{IW}_{jk}|} \times |\text{LW}_j|\right]\right]} \tag{10}$$

Table 4
Comparison of maximum phosphate (as PO_4–P) adsorption capacities (Q_m) of different Ca-containing adsorbents

Material	Initial phosphate concentration	Phosphate adsorption capacity	Reference
	(mg/L)	(mg/g)	
Heated Ca-rich attapulgite	400	5.99	[30]
Ca-imprinted chitosan-supported bentonite	47.67[a]	4.58[a]	[5]
Ca-modified biochar	136.19[a]	35.89[a]	[6]
Ca-activated zeolite	16,000	203.6	[41]
Ca-carbon foam	250	95.27	This study

[a]Converted as phosphate phosphorous (PO_4–P).

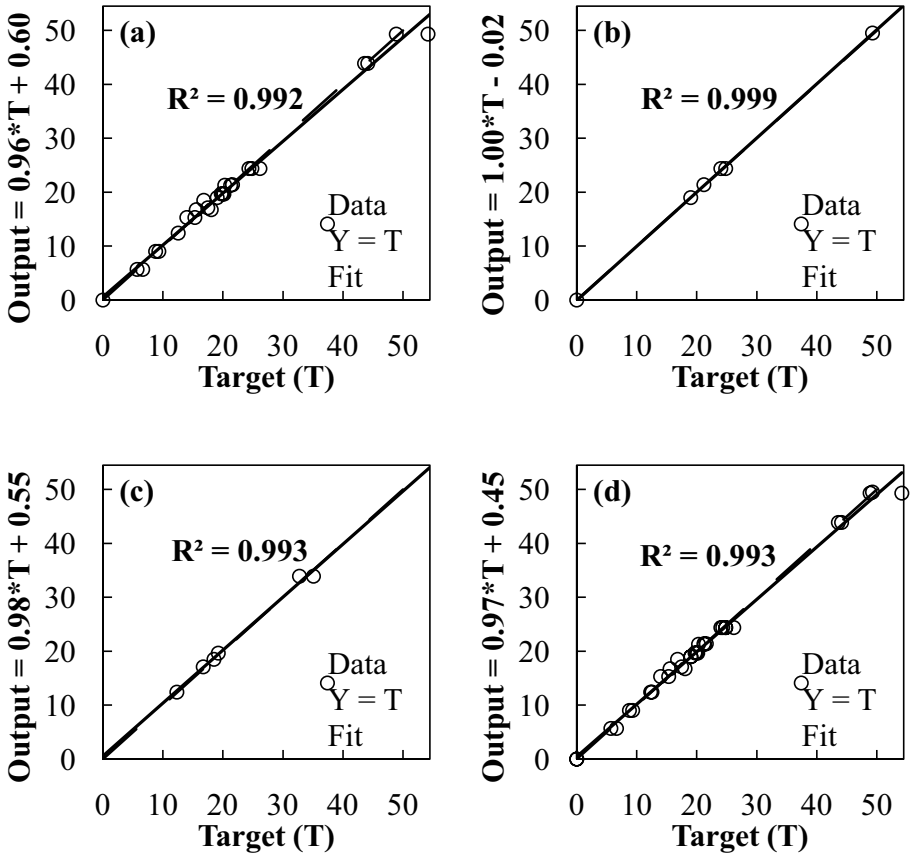

Fig. 7. Scatter plot between experimental data and predicted values of adsorption capacity for (a) training, (b) validation, (c) and testing. (d) Scatter plot between all experimental data and all predicted values of adsorption capacity.

Table 5
Weight and bias values of hidden and output layers of optimal ANN model

IW			LW	b_1	b_2
3.0027	–1.3674	1.8852	0.54443	–3.8014	–0.79694
–2.5777	–0.74495	–2.7469	0.56306	3.327	
–3.0195	–1.6176	1.8843	–0.27793	2.9232	
–0.065563	2.3309	2.7944	–0.76163	2.5825	
2.9863	1.7666	0.07892	–0.26056	–2.5899	
3.0374	–0.44651	2.1286	0.35672	–1.9171	
–2.9406	1.1574	–2.1272	0.41977	1.333	
0.065565	2.8159	2.2163	–0.60394	–1.3341	
2.1278	–1.9392	2.4834	–0.061271	–0.61185	
2.62	–1.7328	2.1313	0.13966	–0.32893	
2.7153	0.74741	–2.2377	–0.60263	–0.2772	
2.2071	2.0299	–2.5081	–0.24661	0.35301	
2.8674	2.4882	0.58241	0.92761	0.47403	
–2.387	–1.3726	–1.0057	–0.9333	–1.8215	
0.29696	–3.8587	–0.034309	0.5235	1.5234	
–1.5999	–2.326	2.3051	0.42145	–2.415	
3.3798	–1.5288	0.36858	–0.032948	2.3292	
2.0671	2.071	2.1742	0.41941	3.2771	
–2.8761	–2.2274	–0.061995	–0.62132	–3.4438	
2.9647	2.2285	–0.51996	0.26962	3.869	

where V is the relative importance of each input parameter, m is the number of neurons in the input layer, h is the number of neurons in the output layer, and i is the number of neurons in the output layer. The relative importance of each input parameter in the ANN model with the trainlm algorithm was calculated using Eq. (10). These results revealed that solution pH (37%) and time (35%) were the most influential parameters for phosphate adsorption on Ca-carbon foam and that the initial phosphate concentration (28%) was less influential than these two parameters.

4. Conclusions

Ca-containing carbon foam was prepared by a simple method and applied to the removal of phosphate from water, and the phosphate adsorption characteristics of the prepared foam were analyzed using kinetic, equilibrium isotherm, and ANN models. The phosphate adsorption capacity of the Ca-containing carbon foam decreased with an increase in solution pH from 3.05 to 6.99 and increased with increases in the time and initial phosphate concentration up to 120 min and 250 mg/L as PO_4–P, respectively. The kinetic and equilibrium data were well described by the pseudo-second-order model and the Freundlich isotherm, which indicate chemisorption and multilayer adsorption, respectively, are involved in phosphate adsorption on Ca-carbon foam. The optimal ANN for the solution pH, initial phosphate concentration, and time in the process of phosphate adsorption on Ca-carbon foam was determined to have a 3–20–1 structure, and among these three parameters, solution pH was found to be most influential. The results of these analyses can be used to design the process of phosphate adsorption on adsorbents for its removal from water.

Acknowledgment

This work was supported by the Ajou University Research Fund.

References

[1] C.G. Lee, P.J.J. Alvarez, H.G. Kim, S. Jeong, S. Lee, K.B. Lee, S.H. Lee, J.W. Choi, Phosphorous recovery from sewage sludge using calcium silicate hydrates, Chemosphere, 193 (2018) 1087–1093.
[2] J.-H. Kim, J.-A. Park, J.-K. Kang, S.-B. Kim, C.-G. Lee, S.-H. Lee, J.-W. Choi, Phosphate sorption to quintinite in aqueous solutions: kinetic, thermodynamic and equilibrium analyses, Environ. Eng. Res., 20 (2015) 73–78.
[3] K. Kang, C.-G. Lee, J.-W. Choi, S.-G. Hong, S.-J. Park, Application of thermally treated crushed concrete granules for the removal of phosphate: a cheap adsorbent with high adsorption capacity, Water Air Soil Pollut., 228 (2016) 8–16.
[4] M.-J. Kim, J.-H. Lee, C.-G. Lee, S.-J. Park, Thermal treatment of attapulgite for phosphate removal: a cheap and natural adsorbent with high adsorption capacity, Desal. Wat. Treat., 114 (2018) 174–184.
[5] I.A. Kumar, N. Viswanathan, Development of multivalent metal ions imprinted chitosan biocomposites for phosphate sorption, Int. J. Biol. Macromol., 104 (2017) 1539–1547.
[6] S.-b. Liu, X.-f. Tan, Y.-g. Liu, Y.-l. Gu, G.-m. Zeng, X.-j. Hu, H. Wang, L. Zhou, L.-h. Jiang, B.-b. Zhao, Production of biochars from Ca impregnated ramie biomass (*Boehmeria nivea* (L.) Gaud.) and their phosphate removal potential, RSC Adv., 6 (2016) 5871–5880.
[7] G. Tondi, V. Fierro, A. Pizzi, A. Celzard, Tannin-based carbon foams, Carbon, 47 (2009) 1480–1492.
[8] M. Emmel, C.G. Aneziris, Development of novel carbon bonded filter compositions for steel melt filtration, Ceram. Int., 38 (2012) 5165–5173.
[9] G. Amaral-Labat, E. Gourdon, V. Fierro, A. Pizzi, A. Celzard, Acoustic properties of cellular vitreous carbon foams, Carbon, 58 (2013) 76–86.
[10] C.G. Lee, J.W. Jeon, M.J. Hwang, K.H. Ahn, C. Park, J.W. Choi, S.H. Lee, Lead and copper removal from aqueous solutions using carbon foam derived from phenol resin, Chemosphere, 130 (2015) 59–65.
[11] C.G. Lee, M.K. Song, J.C. Ryu, C. Park, J.W. Choi, S.H. Lee, Application of carbon foam for heavy metal removal from industrial plating wastewater and toxicity evaluation of the adsorbent, Chemosphere, 153 (2016) 1–9.
[12] C.G. Lee, S. Lee, J.A. Park, C. Park, S.J. Lee, S.B. Kim, B. An, S.T. Yun, S.H. Lee, J.W. Choi, Removal of copper, nickel and chromium mixtures from metal plating wastewater by adsorption with modified carbon foam, Chemosphere, 166 (2017) 203–211.
[13] D.D. Do, Adsorption Analysis: Equilibria and Kinetics, Imperial College Press, London, 1998.
[14] S.S. Gupta, K.G. Bhattacharyya, Kinetics of adsorption of metal ions on inorganic materials: a review, Adv. Colloid Interface Sci., 162 (2011) 39–58.
[15] K.Y. Foo, B.H. Hameed, Insights into the modeling of adsorption isotherm systems, Chem. Eng. J., 156 (2010) 2–10.
[16] R. Han, J. Zhang, P. Han, Y. Wang, Z. Zhao, M. Tang, Study of equilibrium, kinetic and thermodynamic parameters about methylene blue adsorption onto natural zeolite, Chem. Eng. J., 145 (2009) 496–504.
[17] C.-G. Lee, J.-H. Kim, J.-K. Kang, S.-B. Kim, S.-J. Park, S.-H. Lee, J.-W. Choi, Comparative analysis of fixed-bed sorption models using phosphate breakthrough curves in slag filter media, Desal. Wat. Treat., 55 (2014) 1795–1805.
[18] T. Khan, M.R.U. Mustafa, M.H. Isa, T.S.B.A. Manan, Y.-C. Ho, J.-W. Lim, N.Z. Yusof, Artificial neural network (ANN) for modelling adsorption of lead (Pb (II)) from aqueous solution, Water Air Soil Pollut., 228 (2017) 426.
[19] M. Selvanathan, K.T. Yann, C.H. Chung, A. Selvarajoo, S.K. Arumugasamy, V. Sethu, Adsorption of copper(II) ion from aqueous solution using biochar derived from Rambutan (Nepheliumlappaceum) peel: feedforward neural network modelling study, Water Air Soil Pollut., 228 (2017) 299.
[20] J. Ye, X. Cong, P. Zhang, G. Zeng, E. Hoffmann, Y. Wu, H. Zhang, W. Fang, Operational parameter impact and back propagation artificial neural network modeling for phosphate adsorption onto acid-activated neutralized red mud, J. Mol. Liq., 216 (2016) 35–41.
[21] R.M. Aghav, S. Kumar, S.N. Mukherjee, Artificial neural network modeling in competitive adsorption of phenol and resorcinol from water environment using some carbonaceous adsorbents, J. Hazard. Mater., 188 (2011) 67–77.
[22] R. Li, J.J. Wang, B. Zhou, M.K. Awasthi, A. Ali, Z. Zhang, L.A. Gaston, A.H. Lahori, A. Mahar, Enhancing phosphate adsorption by Mg/Al layered double hydroxide functionalized biochar with different Mg/Al ratios, Sci. Total Environ., 559 (2016) 121–129.
[23] W. Huang, J. Chen, F. He, J. Tang, D. Li, Y. Zhu, Y. Zhang, Effective phosphate adsorption by Zr/Al-pillared montmorillonite: insight into equilibrium, kinetics and thermodynamics, Appl. Clay Sci., 104 (2015) 252–260.
[24] W. Xiong, J. Tong, Z. Yang, G. Zeng, Y. Zhou, D. Wang, P. Song, R. Xu, C. Zhang, M. Cheng, Adsorption of phosphate from aqueous solution using iron-zirconium modified activated carbon nanofiber: performance and mechanism, J. Colloid Interface Sci., 493 (2017) 17–23.
[25] J.A. Marshall, B.J. Morton, R. Muhlack, D. Chittleborough, C.W. Kwong, Recovery of phosphate from calcium-containing aqueous solution resulting from biochar-induced calcium phosphate precipitation, J. Cleaner Prod., 165 (2017) 27–35.
[26] S. Shahabuddin, C. Tashakori, M.A. Kamboh, Z.S. Korrani, R. Saidur, H.R. Nodeh, M.E. Bidhendi, Kinetic and equilibrium

adsorption of lead from water using magnetic metformin-substituted SBA-15, Environ. Sci. Water Res. Technol., 4 (2018) 549–558.
[27] C.A. Almeida, N.A. Debacher, A.J. Downs, L. Cottet, C.A. Mello, Removal of methylene blue from colored effluents by adsorption on montmorillonite clay, J. Colloid Interface Sci., 332 (2009) 46–53.
[28] M. Dogan, H. Abak, M. Alkan, Adsorption of methylene blue onto hazelnut shell: kinetics, mechanism and activation parameters, J. Hazard. Mater., 164 (2009) 172–181.
[29] M.A. Al-Ghouti, M.A. Khraisheh, M.N. Ahmad, S. Allen, Adsorption behaviour of methylene blue onto Jordanian diatomite: a kinetic study, J. Hazard. Mater., 165 (2009) 589–598.
[30] H. Yin, X. Yan, X. Gu, Evaluation of thermally-modified calcium-rich attapulgite as a low-cost substrate for rapid phosphorus removal in constructed wetlands, Water Res., 115 (2017) 329–338.
[31] S. Lagergren, Zur Theorie der sogenannten Absorption gelöster Stoffe, P.A. Norstedt & söner, 1898.
[32] Y.-S. Ho, G. McKay, Sorption of dye from aqueous solution by peat, Chem. Eng. J., 70 (1998) 115–124.
[33] J. Zeldowitsch, Über den mechanismus der katalytischen oxydation von CO an MnO2, Acta Physicochim, URSS, 1 (1934) 364–449.
[34] Y.S. Ho, Review of second-order models for adsorption systems, J. Hazard. Mater., 136 (2006) 681–689.
[35] H. Freundlich, Over the adsorption in solution, J. Phys. Chem., 57 (1906) 1100–1107.
[36] I. Langmuir, The adsorption of gases on plane surfaces of glass, mica and platinum, J. Am. Chem. Soc., 40 (1918) 1361–1403.
[37] O. Redlich, D.L. Peterson, A useful adsorption isotherm, J. Phys. Chem., 63 (1959) 1024–1024.
[38] Q. Liu, H. Guo, Y. Shan, Adsorption of fluoride on synthetic siderite from aqueous solution, J. Fluorine Chem., 131 (2010) 635–641.
[39] S.-Y. Yoon, C.-G. Lee, J.-A. Park, J.-H. Kim, S.-B. Kim, S.-H. Lee, J.-W. Choi, Kinetic, equilibrium and thermodynamic studies for phosphate adsorption to magnetic iron oxide nanoparticles, Chem. Eng. J., 236 (2014) 341–347.
[40] L. Zhang, S. Hong, J. He, F. Gan, Y.-S. Ho, Adsorption characteristic studies of phosphorus onto laterite, Desal. Wat. Treat., 25 (2012) 98–105.
[41] M. Hermassi, C. Valderrama, N. Moreno, O. Font, X. Querol, N. Batis, J.L. Cortina, Powdered Ca-activated zeolite for phosphate removal from treated waste-water, J. Chem. Technol. Biotechnol., 91 (2016) 1962–1971.
[42] A. Debnath, K. Deb, K.K. Chattopadhyay, B. Saha, Methyl orange adsorption onto simple chemical route synthesized crystalline α-Fe_2O_3 nanoparticles: kinetic, equilibrium isotherm, and neural network modeling, Desal. Wat. Treat., 57 (2015) 13549–13560.
[43] G.D. Garson, Interpreting neural-network connection weights, AI Expert, 6 (1991) 46–51.